

## NON-GAUSSIAN PDF MODELING OF TURBULENT BOUNDARY LAYER FLUCTUATING PRESSURE EXCITATION

Alexander Steinwolf

The University of Auckland, Department of Mechanical Engineering  
Auckland 1001, New Zealand. Email: [a.steinwolf@auckland.ac.nz](mailto:a.steinwolf@auckland.ac.nz)

Stephen A. Rizzi

NASA Langley Research Center, Structural Acoustics Branch  
Hampton, Virginia 23681-2199, USA. Email: [s.a.rizzi@larc.nasa.gov](mailto:s.a.rizzi@larc.nasa.gov)

### ABSTRACT

The purpose of the study is to investigate properties of the probability density function (PDF) of turbulent boundary layer fluctuating pressures measured on the exterior of a supersonic transport aircraft. It is shown that fluctuating pressure PDFs differ from the Gaussian distribution even for surface conditions having no significant discontinuities. The PDF tails are wider and longer than those of the Gaussian model. For pressure fluctuations upstream of forward-facing step discontinuities and downstream of aft-facing step discontinuities, deviations from the Gaussian model are more significant and the PDFs become asymmetrical. Various analytical PDF distributions are used and further developed to model this behavior.

### INTRODUCTION

Acoustic fatigue of high-speed aircraft structures usually results from elevated acoustic loads near the engines, where overall sound pressure levels often exceed 160 dB. A less common mechanism for high-cycle fatigue is structural response due to turbulent boundary layer pressure fluctuations. This is due to both reduced overall levels (typically in the 130-135 dB range) and short correlation lengths. However, it has been recently shown with data from wind tunnel [1, 2] and flight [3] experiments that the turbulent boundary layer loading can be amplified in excess of 30 dB upstream of small forward-facing step discontinuities and in excess of 20 dB downstream of small aft-facing steps. Thus, near such discontinuities, the loading is such that high-cycle fatigue becomes a concern.

Although it has been shown that a coupling exists between the fluctuating pressure and flexible panels' dynamic response for supersonic conditions [4], fully coupled computations are at-present prohibitive for any practical length scale. Therefore, dynamic response analyses have typically been based on rigid wall pressure models with a weak coupling approximation. Turbulent boundary layer pressure fluctuations are often characterized by a wavenumber-frequency spectrum model, which serves as the forcing function in the absence of fluctuating pressure time histories. A comparison of several models may be found in [5]. The problem with such an approach when considering high-cycle fatigue is that while the calculated dynamic response may be sufficiently accurate in terms of its root-mean-square level and power spectral density, there is no information available regarding the response probability distribution. Lacking that information, the response may be erroneously assumed to have a Gaussian distribution, and one of several spectral-based cycle counting schemes applied [6]. Since most of the fatigue damage results from the high stress ranges, differences in the distribution tails may lead to an inaccurate fatigue life prediction. The characterization of the probability density of the turbulent boundary layer pressure fluctuations is therefore required so that accurate distributions can be used in subsequent fatigue life calculations.

The purposes of the present study are two-fold. One is to investigate properties of boundary layer fluctuating pressure PDFs over a broad range of flight and fuselage surface conditions. The second is to explore the use of, and further develop, analytical expressions capable of modeling the observed PDFs. In this preliminary study, the emphasis is on describing a particular experimental PDF using various analytical expressions. Further, the ease with which such expressions may be used in a structural dynamic response analysis is considered. No attempt was made to parameterize the PDF models with flight and surface conditions. Thus, prediction of the PDF for a particular condition is beyond the scope of this work.

## EXPERIMENT DESCRIPTION

Experimental data acquired from the Tupolev Tu-144LL Supersonic Flying Laboratory [7, 8] was used in this study. Pressure fluctuation time history data were acquired over the length of the fuselage for various subsonic and supersonic flight conditions. On the aircraft starboard side, Kulite pressure transducers (model XCS-190-15D) were flush mounted in window blanks (WB) and fuselage sidewall locations as indicated in [7]. These transducers were used to measure pressure fluctuations on the smooth sidewall. Measurements at three window blank locations were considered in this paper;  $\sim 18.9\text{m}$  (transducer N1.1, WB1),  $\sim 32.6\text{m}$  (N4.1, WB 4), and  $\sim 49.3\text{m}$  (N7.2, WB 7) from the aircraft nose (including the nose boom).

On the port side of the aircraft, step plates were installed on the fuselage exterior at two locations spanning adjacent window blanks, see Figure 1. The forward plate was in a longitudinal location close to and opposite transducer N1.1. The rear plate location was located close to and opposite transducer N7.2. The approximate distances of the port-side window blanks from the aircraft nose were:  $\sim 21.7\text{m}$ ,  $\sim 22.6\text{m}$ ,  $\sim 44.9\text{m}$ , and  $\sim 45.8\text{m}$ , for window blanks 8, 9, 10 and 11, respectively. Within window blanks 8-11 (see Figure 2), miniature Kulite pressure transducers (model XCS-062-15D) were flush mounted, as described in [8]. Transducers in window blanks 8 and 10 were exposed to the effects of a forward facing step, while those in window blanks 9 and 11 were exposed to the effects of an aft facing step. The step plates were comprised of two layered plates measuring 4 and 3 mm in height. For flights 24-26, both plates were used to achieve a total step height of 7 mm. For flight 27, the upper 3 mm plate was removed leaving a step height of 4 mm.

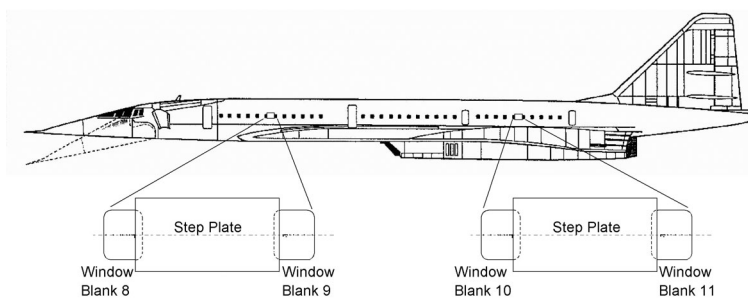


*Figure 1: Location and identification of window blanks instruments in vicinity of step plates.*

All transducer faces were flush mounted with respect to the neighboring window blank material and the fuselage sidewall. Flushness measurements are documented in [7, 8]. Independent signal conditioning of each transducer was provided to allow for simultaneous measurements. Signals were AC coupled to remove the static differential pressure across the fuselage sidewall at altitude. Anti-aliasing filters were applied at a corner frequency of 11.2 kHz (the upper frequency of the 10 kHz 1/3-octave band). A digital recorder was used to record long, contiguous time histories of the data, typically between 30-60 seconds each.

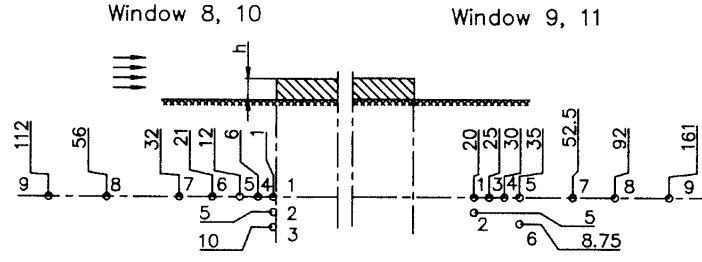


Figure 2: Layout of measurement points in front of forward-facing steps and behind aft-facing steps. Dimensions are in mm.

### EXPERIMENTAL PDF, SKEWNESS AND KURTOSIS CHARACTERISTICS

The analysis of experimental data concentrated on determination of the PDF and calculation of skewness and kurtosis characteristics. Skewness,  $\lambda$ , and kurtosis,  $\gamma$ , are the principal parameters describing non-Gaussian PDF features and are defined as

$$\lambda = \frac{E[(u-m)^3]}{\sigma^3}, \quad \gamma = \frac{E[(u-m)^4]}{\sigma^4} \quad (1)$$

where  $u$  is the random variable (in this case the fluctuating pressure),  $m$  is the mean value of  $u$ ,  $E[.]$  is the expected value, and  $\sigma$  is the standard deviation of  $u$ . The PDF of a random variable  $u$  with a Gaussian distribution is written as

$$P_G(u) = \frac{1}{\sigma\sqrt{2\pi}} e^{-\frac{(u-m)^2}{2\sigma^2}} \quad (2)$$

For the Gaussian random process, the skewness is 0 and kurtosis is 3. If the experimental PDF is non-Gaussian, but symmetric with respect to the mean, kurtosis is the only additional parameter required to describe the distribution. It characterizes the sharpness or flatness of the PDF peak and the wideness or narrowness of the PDF tails. A kurtosis value greater than 3 indicates a sharper peak and wider tail than the Gaussian PDF. If the experimental PDF is asymmetrical with respect to the mean, then the skewness is non-zero and its sign will indicate the direction in which the PDF is skewed.

For time history analysis, the crest factor,  $c$ , can serve as another indicator of non-Gaussian behavior. The crest factor is related to the PDF tails and is defined as the ratio between the highest time history peak and the signal root-mean-square value. While this parameter is more intuitive and easier to calculate than kurtosis, it is of limited value, as its magnitude increases with increasing data record length.

**Results for the smooth surface.** Kurtosis values for the smooth surface condition (no step) are shown in Table 1 for one subsonic and three supersonic flight conditions. The run numbers are provided to serve as a cross-reference to additional flight data provided in [8]. For each smooth surface condition, reported kurtosis values were obtained by averaging the individual kurtosis values from the two runs indicated, each at three transducer locations (N1.1, N4.1 and N7.2). It is readily noted from the kurtosis that the data exhibits non-Gaussian behavior. The subsonic condition had the highest kurtosis value of 4.1, while the highest supersonic condition at Mach 2.0 had the lowest kurtosis value of 3.7. The

variation of kurtosis along the length of the fuselage was insignificant ( $< 0.2$ ). The skewness was negligible for all subsonic and supersonic flight conditions.

Plots of typical PDFs for the subsonic and Mach 2.0 conditions are shown in Figure 3 – Figure 6 along with the Gaussian model. The data is plotted on a linear scale to show the distribution at the peak, and on a semi-log scale to show the PDF tails. The experimental PDFs are taller and sharper than the Gaussian model at the peak, see Figure 3 and Figure 5. More importantly, the experimental PDF tails are much wider than those of the Gaussian model, see Figure 4 and Figure 6. In other words, the probability of a high peak occurrence in the experimental data is several times larger than that predicted by the Gaussian model. From a structural dynamics standpoint, any synthetic time history of this loading generated using the Gaussian model will under represent the number of high peak events relative to the experimental data. In terms of crest factor, the subsonic condition reached a value of 10.0 for the subsonic condition and 9.0 for the supersonic conditions. By comparison, the crest factor for records of similar length for a Gaussian process would be roughly 4.5 – 5.0.

*Table 1: Kurtosis and skewness of fluctuating pressure upstream of forward-facing steps.*

Run No.	Aircraft Mach No./ Alt (km)	Step Height (mm)	Window Blank No.	Kurtosis/skewness (Smooth)	Kurtosis/skewness upstream of forward facing steps at distance of:			
					112 mm (Xdcr 9)	56 mm (Xdcr 8)	32 mm (Xdcr 7)	1 mm (Xdcr 1)
(†)	0.75 / 4.9	0	Avg	4.1 / 0.1				
194		4	8		4.2 / 0	3.8 / 0.2	3.4 / 0.3	3.6 / 0.3
195		4	10		4.1 / 0.1	3.5 / 0.2	3.4 / <b>0.4</b>	3.4 / <b>0.4</b>
122		7	8		4.0 / 0.1	3.5 / 0.2	3.4 / <b>0.4</b>	4.0 / <b>0.7</b>
124		7	10		3.9 / 0.1	3.3 / 0.3	3.3 / <b>0.4</b>	n/a
(‡)	1.2 / 12.0	0	Avg	3.9 / 0.1				
187		4	8		3.8 / 0	3.4 / 0.1	3.3 / <b>0.4</b>	3.6 / <b>0.5</b>
188		4	10		3.3 / 0	3.2 / 0.2	3.3 / <b>0.4</b>	3.7 / <b>0.6</b>
152		7	8		3.6 / 0	3.3 / 0.2	3.3 / <b>0.4</b>	<b>4.4 / 0.9</b>
151		7	10		3.3 / 0	3.2 / 0.2	3.2 / <b>0.4</b>	<b>4.6 / 1.0</b>
(*)	1.6 / 14.0	0	Avg	3.8 / 0				
183		4	8		3.6 / -0.1	3.8 / <b>-0.6</b>	3.2 / 0.2	3.8 / <b>0.7</b>
184		4	10		3.5 / 0	3.1 / <b>-0.6</b>	3.1 / 0.1	3.9 / <b>0.7</b>
149		7	8		3.6 / 0.3	3.6 / 0.2	3.3 / 0.2	<b>5.0 / 1.1</b>
148		7	10		3.6 / 0.3	3.6 / 0.1	3.2 / 0.2	<b>5.0 / 1.1</b>
(#)	2.0 / 16.7	0	Avg	3.7 / 0				
180		4	8		3.6 / -0.1	<b>4.3 / 0.7</b>	<b>7.3 / -1.4</b>	<b>5.3 / 0.7</b>
181		4	10		3.3 / 0	<b>4.4 / 0.7</b>	<b>5.7 / -1.3</b>	<b>5.4 / 0.8</b>
165		7	8		3.6 / -0.1	4.1 / <b>-0.9</b>	3.3 / 0.1	3.8 / <b>1.2</b>
167		7	10		3.3 / 0	3.1 / <b>-0.7</b>	3.2 / 0	4.0 / <b>1.2</b>

(†) Runs 123 & 196, (‡) Runs 153 & 189, (\*) Runs 150 & 185, (#) Runs 166 & 182

**Results for surfaces with forward-facing step discontinuities.** Power spectral density data from the surface condition with small step discontinuities were previously studied in [1-3]. The PDF analysis of such flight data is new. The qualitative difference between the PDFs obtained from the smooth surface and the stepped surface conditions is that the latter becomes skewed.

Figure 7 – Figure 10 show PDF peaks and tails for the run 165 forward-facing step condition, see Table 1. Immediately in front of the step, Figure 7 shows a positive skewness, giving a PDF peak shifted in the negative direction. The corresponding PDF tail, Figure 8, is much longer in the positive direction than in the negative direction. At a point further upstream, Figure 9 shows a negative skewness, giving a PDF peak shifted in the positive direction, with a somewhat longer tail in the negative direction than in the positive direction, see Figure 10. The effect of skewness is clearly demonstrated in the fluctuating pressure time history 1mm upstream of the forward-facing step, see Figure 11. It is less striking, but still apparent in the pressure time history 56mm upstream of the forward-facing step, see Figure 12.

Kurtosis and skewness data for the forward facing step condition is shown in Table 1 for one subsonic and three supersonic flight conditions. The most significant deviations from Gaussian are highlighted in bold. As expected, the analyses show that the intensity of non-Gaussian behavior depends on the distance from the step. Data from transducers located at 112 mm before the step (8.9 and 10.9) indicate no notable differences compared to the smooth surface data. The skewness values are nearly zero and kurtosis values were close to those of the smooth surface, though perhaps a bit smaller in the supersonic regime. This indicates that beyond a particular point in front of the forward facing step, the effect of the step does not further influence the non-Gaussian parameters of the fluctuating pressure.

As the proximity to the step increases, the effect on the non-Gaussian parameters becomes more significant and strongly influenced by step height. Consider, for example, the 4mm step data at Mach 2.0 (runs 180 and 181). In these cases, the kurtosis peaks at a distance of 32 mm (at transducers 8.7 and 10.7). The skewness distribution as a function of distance from the step exhibits an oscillatory pattern. Proceeding from 112mm to 1mm, the skewness is near zero, is positive at 56mm, negative at 32 mm, then again positive at 1mm. What is interesting is that both the skewness and kurtosis follow identical patterns, with nearly identical values of skewness at the forward (run 180) and the aft (run 181) fuselage locations. This indicates insensitivity of the non-Gaussian parameters to location on the aircraft, which may be loosely interpreted as insensitivity to Reynold's number and boundary layer thickness. Skewness and kurtosis from the two Mach 2.0 runs with a 7mm step (165 and 167) exhibit similar characteristics to each other, but those characteristics differ from the 4 mm step height. Interpretation of these non-Gaussian behaviors in terms of the flow physics is beyond the scope of this paper.

As the Mach number is decreased from 2.0 to 0.75, the character of the non-Gaussian behavior is additionally affected. Compare, for example, the skewness and kurtosis for the 4mm step in the rear location as a function of Mach number (runs 181, 184, 188 and 195). As the Mach number decreases, the oscillation wavelength of the skewness distribution appears to increase and the oscillation amplitude of the skewness distribution decreases. Further, the kurtosis variation with distance from the step becomes smoother, and in the subsonic case does not exceed that of the smooth surface condition. As with the Mach 2 condition, the similarity between non-Gaussian behaviors at forward (window blank 8) and rear (window blank 10) positions is maintained for a given step height, and varies with differing step height for the other flight regimes.

**Results for surfaces with aft-facing step discontinuities.** Kurtosis and skewness for positions downstream of aft-facing step discontinuities are presented in Table 2. This data does not exhibit as strong a pattern of behavior with distance from the step and across flight regimes as the forward facing step. Any such patterns are both different and subtle.

Table 2: Kurtosis and skewness of fluctuating pressure downstream of aft-facing steps.

Run No.	Aircraft Mach No./ Alt (km)	Step Height (mm)	Window Blank No.	Kurtosis/skewness downstream of aft facing steps at distance of:		
				20 mm (Xdcr 1)	52.5 mm (Xdcr 7)	161 mm (Xdcr 9)
194	0.75 / 4.9	4	9	3.6 / 0.2	3.7 / 0.1	4.1 / -0.1
195		4	11	3.6 / 0.1	3.7 / 0.2	4.0 / 0.2
122		7	9	3.6 / <b>-0.4</b>	3.6 / 0.2	4.1 / -0.2
124		7	11	3.8 / <b>-0.5</b>	3.5 / 0.1	3.9 / 0.1
187	1.2 / 12.0	4	9	3.3 / 0	3.6 / 0.2	3.8 / -0.1
188		4	11	3.2 / 0	3.5 / 0.1	3.6 / 0.2
152		7	9	3.3 / -0.3	3.4 / 0.2	3.7 / -0.1
151		7	11	3.2 / -0.3	3.2 / 0.2	3.5 / 0.2
183	1.6 / 14.0	4	9	3.2 / 0.3	3.4 / 0.1	3.4 / 0.3
184		4	11	3.2 / 0.3	3.3 / 0.1	3.4 / 0.2
149		7	9	3.3 / 0	3.1 / 0.1	3.5 / 0.2
148		7	11	3.2 / 0	3.2 / 0.1	3.3 / 0.2
180	2.0 / 16.7	4	9	3.1 / 0.2	3.3 / 0.1	3.2 / 0.1
181		4	11	3.0 / 0.1	3.3 / 0	3.4 / 0.2
165		7	9	3.4 / 0.3	3.2 / 0	3.3 / 0.2
167		7	11	3.7 / <b>0.5</b>	3.2 / 0	3.3 / 0.2

Kurtosis values are generally lower than those of the smooth surface condition. At Mach 0.75 and at Mach 1.2, the kurtosis generally increases in value with increasing distance downstream of the step. This tendency is reduced at Mach 1.6, and is not evident at Mach 2.0. Skewness values are mainly within  $\pm 0.2$ , a level which can be considered indistinguishable from the Gaussian behavior. Only at the closest location of 20 mm are greater positive and negative magnitudes ( $\pm 0.5$ ) evident. For a given step height, skewness and kurtosis exhibit similar magnitudes and trends in forward and rear fuselage locations.

To summarize, the non-Gaussian behaviors of fluctuating pressure upstream of forward-facing step discontinuities is highly dependent upon distance from the step and the step height. The behavior is less dependent on aircraft speed, and shows no dependency on location on the fuselage. These observations also apply to the non-Gaussian behaviors downstream of aft-facing steps, however these effects are subtle and both spatial distribution and amplitude differ from those of the forward-facing steps.

### **NON-GAUSSIAN MODELS FOR ANALYTICAL APPROXIMATION OF EXPERIMENTAL PROBABILITY DISTRIBUTIONS**

Non-Gaussian behavior of fluctuating pressure PDFs is evident from the results presented in the previous section. The difference between experimental probability distributions and the Gaussian analytical distribution (2) was quantitative and significant. Hence, no appropriate approximation can be achieved by use of the Gaussian model. Other models able to account for various skewness and kurtosis values are necessary. Several are considered herein, including the Gram-Charlie series, the Hermite polynomial transformation, and a piecewise-Gaussian approximation. A summary of each approximation follows.

**Gram-Charlie Series.** The expansion of the Gaussian PDF (2) into a truncated series has been widely used in the area of dynamics and vibrations [9, 10]. One form, the Gram-Charlie series, may be written as

$$P_{GC}(u) = \frac{1}{\sigma\sqrt{2\pi}} e^{\left(-\frac{\tilde{u}^2}{2}\right)} \left[ 1 + \frac{\lambda}{6} \tilde{u}(\tilde{u}^2 - 3) + \frac{\gamma - 3}{24} (\tilde{u}^4 - 6\tilde{u}^2 + 3) \right] \quad (3)$$

where  $\tilde{u} = (u - m)/\sigma$  is a standardized non-dimensional variable. Because the Gram-Charlie series is truncated, its use is problematic in that it can lead to inappropriate values of the PDF for certain distribution ranges. It has been found [11, 12] that the most critical situation is when the kurtosis value  $\gamma$  is less than 3, giving rise to non-physical negative values of the PDF. Although the fluctuating pressure data presented has  $\gamma > 3$ , another condition occurs for particular values of the last summand in (3), which gives rise to valleys on both sides of the distribution near the argument values  $|u - m| = \sqrt{3}\sigma$ . For skewed distributions, this effect appears for smaller kurtosis values than for non-skewed distributions, the valleys are asymmetric, and have different widths. This behavior is not appropriate for the experimental distributions under consideration, as there is no indication of additional peaks (or valleys) in the tail areas. Clearly, the form of the Gram-Charlie series is easy to implement, however, it cannot be applied without these special considerations.

**Hermite Polynomial Transformation.** To overcome drawbacks of the Gram-Charlie series, a functional transformation of the Gaussian random variable employing Hermite polynomials was developed [13]. This method avoids erroneous negative distribution values by applying Hermite functions to the time history itself, not to the PDF. In doing so, however, its functional form and application become much more complicated. For the 4<sup>th</sup> order Hermite series, the PDF takes the form

$$P_H(u) = \frac{1}{k\sigma\sqrt{2\pi}} \frac{e^{\left(-\frac{v^2}{2}\right)}}{(3h_4v^2 + 2h_3v + 1 - 3h_4)} \quad (4)$$

where

$$v(u) = \left[ \sqrt{\xi^2(u) + c} + \xi(u) \right]^{\frac{1}{3}} - \left[ \sqrt{\xi^2(u) + c} - \xi(u) \right]^{\frac{1}{3}} - a$$

$$\xi(u) = 1.5b \left[ a + (u - m)/(k\sigma) \right] - a^3, \quad b = \frac{1}{3h_4}, \quad a = bh_3, \quad c = (b - 1 - a^2)^3 \quad (5)$$

$$h_3 = \frac{\lambda}{4 + 2\sqrt{1 + 1.5(\gamma - 3)}}, \quad h_4 = \frac{\sqrt{1 + 1.5(\gamma - 3)} - 1}{18}, \quad k = \frac{1}{\sqrt{1 + 2h_3^2 + 6h_4^2}}$$

**Symmetric Piecewise-Gaussian Approximation.** As an alternative to the above methods, a piecewise-Gaussian model has been proposed [14, 15]. The idea of this approach is to construct non-Gaussian PDFs from a few sections of Gaussian distributions (2), each with different parameters. This can be done in such a way as to avoid negative values of the probability density and ensure its unimodality. Such an approach is more flexible in data fitting than the simple Gaussian distribution, but its use is no more complicated than that of the Gaussian model because the piecewise-Gaussian approximation simply entails application

of the Gaussian model (2) several times. Two types of approximations are considered; Type I as previously formulated [15], and a new formulation (Type II), which allows for wider tails.

The Type I formulation for symmetrical ( $\lambda = 0$ ), centralized ( $m = 0$ ), non-Gaussian distribution with variable kurtosis has been composed [15] from two quasi-Gaussian exponential functions with different standard deviations  $\sigma_1$  and  $\sigma_2$

$$P'_s(u) = \begin{cases} Q \left\{ \exp\left[-u^2/2\sigma_1^2\right] + H \right\}, & |u| \leq v \\ Q \exp\left[-(|u| + \sigma_2 - v)^2/2\sigma_2^2\right], & |u| > v \end{cases} \quad (6)$$

All sections of this piecewise-Gaussian PDF were joined in such a way that conditions of continuity for the function  $P_s(u)$  itself and for its derivative were preserved. Note that since the quasi-Gaussian tails were shifted horizontally, the Type I formulation never acquires negative values and thus retains that property of the Gaussian distribution (2). This is an advantage over the Gram-Charlie series. The five parameters  $Q$ ,  $H$ ,  $\sigma_1$ ,  $\sigma_2$ , and  $v$  in (6) may be expressed in terms of the original standard deviation  $\sigma$  and the non-Gaussian parameter  $\beta$ . The parameter  $\beta$  imparts the particular value of kurtosis  $\gamma$  via a nonlinear algebraic equation.

It appeared that the fluctuating pressure PDF tails for the smooth surface condition with symmetric distribution were wider than those that could be provided by the Type I formulation. Since the Type I form does not permit kurtosis values larger than a certain boundary value, an alternative form (Type II) was developed. In the Type II formulation, the exponential functions that made up the Type I form were multiplied by additional factors, which are inversely proportional to  $\sigma_1$  and  $\sigma_2$ . This action changed the equations for determination of the piecewise-Gaussian parameters, and in particular, the relation between  $\beta$  and the specified value of kurtosis  $\gamma$ . In doing so, the range of possible specified kurtosis values was extended, allowing for the creation of analytical PDFs with wider tails than were possible with the Type I form. The Type II formulation for symmetrical ( $\lambda = 0$ ), centralized ( $m = 0$ ), non-Gaussian distribution with variable kurtosis and standard deviation  $\sigma$  is written as

$$P''_s(u, \sigma, \beta) = \begin{cases} \frac{CY}{\sigma\sqrt{2\pi}} \left[ \exp\left(-\frac{u^2}{2\sigma^2\beta^2}\right) + H \right], & |u| \leq \beta B\sigma \\ \frac{C}{\sigma\sqrt{2\pi}} \exp\left\{-\frac{[|u| + \sigma B(Y - \beta)]^2}{2\sigma^2 Y^2 B^2}\right\}, & |u| > \beta B\sigma \end{cases} \quad (7)$$

where

$$H(\beta) = \frac{1}{Y\sqrt{e}} - e^{\left(-\frac{\beta^2}{2}\right)}, \quad C(\beta) = \frac{1}{Y} \sqrt{\frac{\pi}{2}} \frac{1}{DB}, \quad Y(\beta) = \sqrt{\frac{1}{\beta}} e^{\left(\frac{\beta^2-1}{2}\right)}$$

$$B(\beta) = \sqrt{D} \left\{ \beta^3 \frac{H}{3} + \Phi(\beta) - \beta e^{\left(-\frac{\beta^2}{2}\right)} + \left[ \sqrt{\frac{\pi}{2}} - \Phi(1) \right] (2Y^2 - 2\beta Y + \beta^2) + \frac{Y(2\beta - Y)}{\sqrt{e}} \right\}^{-1/2}$$

$$D(\beta) = \beta H + \Phi(\beta) + \sqrt{\frac{\pi}{2}} - \Phi(1), \quad \Phi(\beta) = \int_0^\beta e^{\left(-\frac{\omega^2}{2}\right)} d\omega \quad (8)$$

and the equation for  $\beta$  is as follows

$$\begin{aligned} \beta^5 \frac{H}{5} - \beta(\beta^2 + 3)e^{\left(-\frac{\beta^2}{2}\right)} + \frac{4Y^4 - 12Y^3(Y - \beta) + 6Y^2(Y - \beta)^2 - 4Y(Y - \beta)^3}{\sqrt{e}} \\ + 3\Phi(\beta) + \left[ \sqrt{\frac{\pi}{2}} - \Phi(1) \right] \left[ 3Y^4 + 6Y^2(Y - \beta)^2 + (Y - \beta)^4 \right] = \frac{D}{B^4} \gamma \end{aligned} \quad (9)$$

**Non-Symmetric Piecewise-Gaussian Approximation.** It has been shown [14, 15] that a non-symmetric form of a piecewise-Gaussian model may be constructed from two sections of different symmetric piecewise-Gaussian models joined at the mode value  $\mu$ , the point of peak PDF. That is, the negative side of one symmetric piecewise-Gaussian model is joined with the positive side of another. To ensure smoothness of the function at the mode value, both halves must have the same value of the symmetric non-Gaussian parameter  $\beta$ . An additional equation similar to (9) imparts the desired skewness. Thus far, only the Type I non-symmetric piecewise-Gaussian approximation has been developed. It has the form

$$P'_A(u) = \begin{cases} Q_A \exp\left[-(u - \mu - \sigma_{2L} + v_L)^2 / 2\sigma_{2L}^2\right], & u \leq \mu - v_L \\ Q_A \left\{ \exp\left[-(u - \mu)^2 / 2\sigma_{1L}^2\right] + H_L \right\}, & \mu - v_L < u \leq \mu \\ Q_A \left\{ \exp\left[-(u - \mu)^2 / 2\sigma_{1R}^2\right] + H_R \right\}, & \mu < u \leq \mu + v_R \\ Q_A \exp\left[-(u - \mu + \sigma_{2R} - v_R)^2 / 2\sigma_{2R}^2\right], & u > \mu + v_R \end{cases} \quad (10)$$

Additional details regarding this formulation may be found in [15].

## COMPARISON OF MODELS WITH EXPERIMENTAL DISTRIBUTIONS

**Smooth Surface (Symmetric PDF Case).** All three models were exercised for the smooth surface condition previously shown, using the kurtosis value for that particular condition and skewness of zero. The symmetric Gram-Charlie series approximation (3), shown in Figure 13 gave a little improvement in both the peak and tail compared to the Gaussian approximation shown in Figure 4. If one tries to make the tails of the Gram-Charlie series approximation wider by increasing the kurtosis (in this case to 7), the distribution changes dramatically and in an unacceptable manner, as discussed earlier and as shown in Figure 13. The Type I symmetric piecewise-Gaussian approximation (6), shown in Figure 14, improved both the peak and the tail compared to the Gaussian model. The Type II symmetric piecewise-Gaussian approximation (7) is also shown in Figure 14. It is seen that the Type II formulation more accurately captures the behavior of the PDF tails, albeit at some compromise to the peak.

Lastly, the Hermite polynomial transformation approximation (4) is seen in Figure 15 to agree very well with the experimental distribution. With skewness  $\lambda$  set to zero, equations (5) simplify because  $h_3$  and  $a$  become zero. Even in this form, however, the Hermite polynomial

approximation equations are complicated and hence, their further analytical manipulation is difficult. This is considered a drawback compared with the piecewise-Gaussian models.

**Surface with step discontinuities (Skewed PDF Case).** The Mach 2.0, 7mm forward-facing step condition (run 165) shown in Figure 7 and Figure 8 was used to assess the ability of the three non-symmetric approximations to model experimental data. The skewness and kurtosis used in the models is that of run 165, see Table 1. The Gram-Charlie approximation showed some shift of the peak to the left (see Figure 16), but this is accompanied by improper changes in the form of valleys and peaks of the PDF for positive ranges. Furthermore, the approximation erroneously indicates negative probability distributions in the range of  $-3000$  to  $-4000$  Pa, see Figure 17. Hence, the Gram-Charlie series approximation is unsatisfactory. The more sophisticated non-symmetric Type I piecewise-Gaussian and Hermite polynomials models were more successful. Figure 18 shows that the PDF peak was captured nearly perfectly using the piecewise-Gaussian model, and was also modeled well using the Hermite polynomial model, see Figure 20. There are some differences in the tails, but both models generally reflected the asymmetrical shape. The piecewise-Gaussian model worked somewhat better at the negative tail (Figure 19) whereas the Hermite polynomial model was more precise at the positive tail (Figure 21).

## CONCLUSIONS

In this study, turbulent boundary layer pressure fluctuations from the Tu-144LL were observed to deviate from the Gaussian distribution under all flight conditions. Differences were concentrated mainly at the distribution tails. For the smooth wall condition, skewness was near zero and only the kurtosis was affected. The non-Gaussian behaviors of fluctuating pressure near forward- and aft-facing step discontinuities were additionally skewed and shown to be highly dependent upon the distance from the step and the step height, less dependent on aircraft speed than with distance from step/step height, and not dependent on the fuselage location. The behaviors of points upstream of forward-facing steps appeared more affected than points downstream of aft-facing steps, for the locations considered.

Several approximate models were evaluated including the Gram-Charlie series, Hermite polynomial transformation, and piecewise-Gaussian approximations. Application of the Gram-Charlie series was shown to be problematic both for smooth and stepped wall conditions as non-physical behaviors could be produced under some circumstances. The Hermite polynomial transformation approximation modeled both the smooth wall (symmetric) and forward-facing step (asymmetric) behaviors well. However, its form is not conducive to further analytical manipulation. The piecewise-Gaussian approximations generally worked well, and a new form was developed which allowed for higher values of kurtosis. The advantage of the piecewise-Gaussian models is that when properly constructed from two or four sections having different parameters, their subsequent use requires nothing more than recurring manipulation with the Gaussian model. From a practical standpoint, this allows previously developed Gaussian solutions to be employed in situations in which the PDF is non-Gaussian.

Areas of remaining interest lie in the further development of approximate models (e.g. an asymmetric version of the type II piecewise-Gaussian approximation) and the development of a model to determine skewness and kurtosis for a particular flight condition, step size, and distance from the step. Finally, the effects of a non-Gaussian fluctuating pressure on the fuselage structural dynamic response and fatigue life remain to be assessed.

## REFERENCES

- [1] Efimtsov, B.M., Kozlov, N.M., Kravchenko, S.V., and Andersson, A.O., "Wall pressure-fluctuation spectra at small forward-facing steps," *Proceedings of the 5th AIAA/CEAS Aeroacoustics Conference*, AIAA-99-1964, Bellevue, WA, 1999.
- [2] Efimtsov, B.M., Kozlov, N.M., Kravchenko, S.V., and Andersson, A.O., "Wall pressure-fluctuation spectra at small backward-facing steps," *Proceedings of the 6th AIAA/CEAS Aeroacoustics Conference*, AIAA-2000-2053, Lahaina, HI, 2000.
- [3] Efimtsov, B.M., Golubev, A.Y., Rizzi, S.A., Andersson, A.O., Rackl, R.G., and Andrianov, E.V., "[Influence of small steps on wall pressure fluctuation spectra measured on TU-144LL flying laboratory](#)," *Proceedings of the 8th AIAA/CEAS Aeroacoustics Conference*, AIAA-2002-2605, Breckenridge, CO, 2002.
- [4] Frendi, A., "Coupling between a supersonic turbulent boundary layer and a flexible structure," *AIAA Journal*, Vol. 35, No. 1, pp. 58-66, 1997.
- [5] Graham, W.R., "A comparison of models for the wavenumber-frequency spectrum of turbulent boundary layer pressures," *Journal of Sound and Vibration*, Vol. 206, No. 4, pp. 541-565, 1997.
- [6] Bouyssy, V., Naboishikov, S.M., and Rackwitz, R., "Comparison of analytical counting methods for Gaussian processes," *Structural Safety*, Vol. 12, pp. 35-57, 1993.
- [7] Rizzi, S.A., Rackl, R.G., and Andrianov, E.V., "[Flight test measurements from the Tu-144LL structure/cabin noise experiment](#)," NASA TM-2000-209858, January 2000.
- [8] Rizzi, S.A., Rackl, R.G., and Andrianov, E.V., "[Flight test measurements from the Tu-144LL structure/cabin noise follow-on experiment](#)," NASA TM-2000-209859, February 2000.
- [9] Crandall, S.H., "Non-Gaussian closure for random vibration of non-linear oscillators," *International Journal of Non-Linear Mechanics*, Vol. 15, pp. 303-313, 1980.
- [10] Melzer, H.J. and Schueller, G.J., "On the reliability of flexible structures under non-normal loading processes," *Proceedings of IUTAM Symposium on Random Vibration and Reliability*, Akademie-Verlag, pp. 73-83, Frankfurt/Oder, 1983.
- [11] Barton, D.E. and Dennis, K.E., "The conditions under which Gram-Charlie and Edgeworth curves are positive definite and unimodal," *Biometrika*, Vol. 39, pp. 425-427, 1952.
- [12] Steinwolf, A., Ferguson, N.S., and White, R.G., "Variations in steepness of the probability density function of beam random vibration," *European Journal of Mechanics A/Solids*, Vol. 19, pp. 319-341, 2000.
- [13] Winterstein, S.R., "Nonlinear vibration models for extremes and fatigue," *ASCE Journal of Engineering Mechanics*, Vol. 114, pp. 1772-1790, 1988.
- [14] Steinwolf, A., "Analysis and simulation of non-Gaussian random vibrations," Naukova Dumka, Kiev (in Russian), 1993.
- [15] Steinwolf, A., "Analysis and approximation of probability distribution of vehicle random vibrations with consideration of kurtosis and skewness values," *Structural Dynamics: Recent Advances, Proceedings of the 5th International Conference*, Vol. 2, pp. 785-794, Southampton, England, 1994.

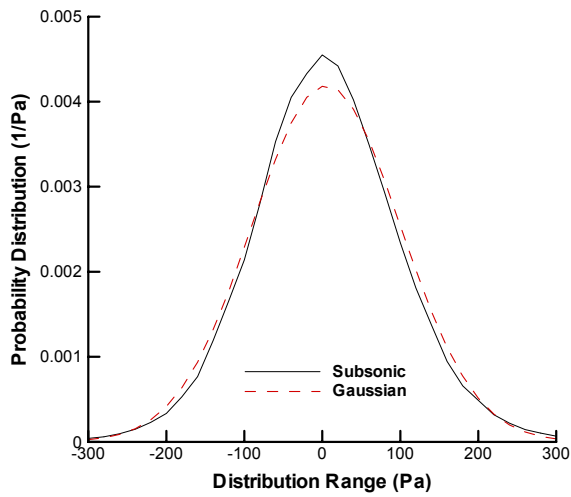


Figure 3: PDF peak of fluctuating pressure from smooth surface (subsonic).

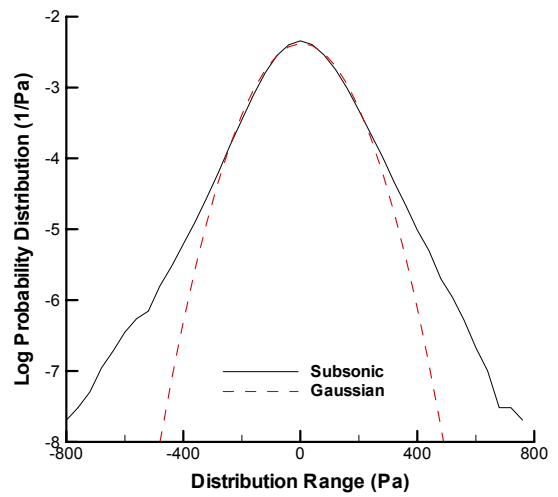


Figure 4: PDF tail of fluctuating pressure from smooth surface (subsonic).

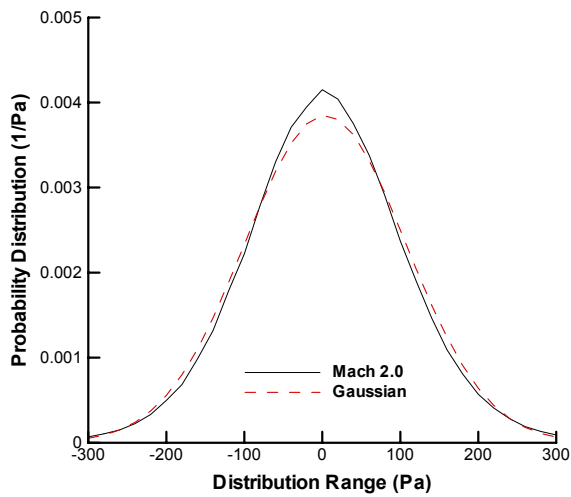


Figure 5: PDF peak of fluctuating pressure from smooth surface (M 2.0).

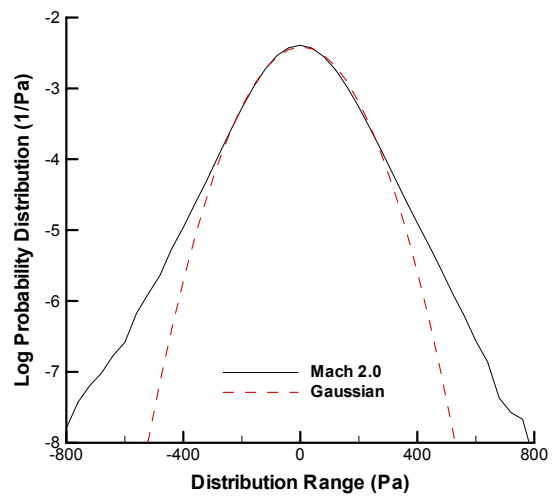


Figure 6: PDF tail of fluctuating pressure from smooth surface (M 2.0).

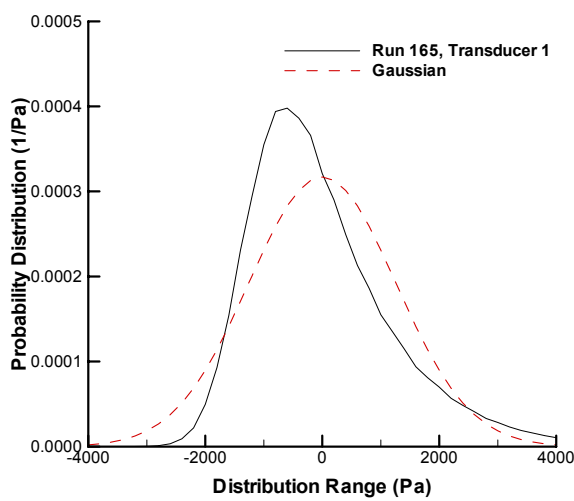


Figure 7: PDF peak of fluctuating pressure at 1mm upstream of forward-facing step.

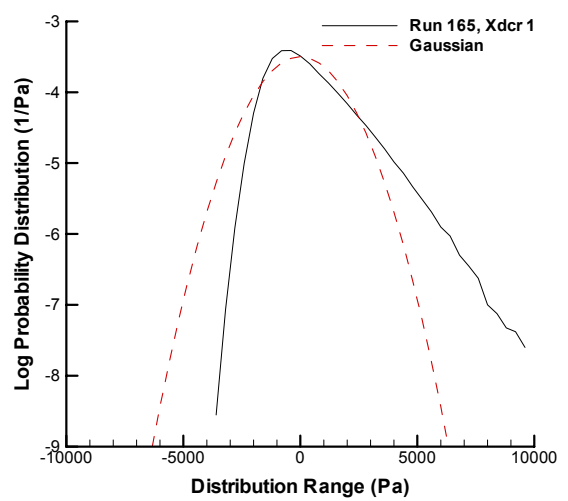


Figure 8: PDF tail of fluctuating pressure at 1mm upstream of forward-facing step.

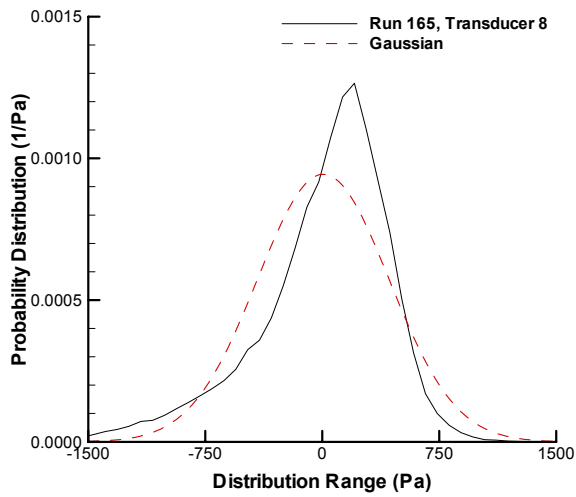


Figure 9: PDF peak of fluctuating pressure at 56mm upstream of forward-facing step.

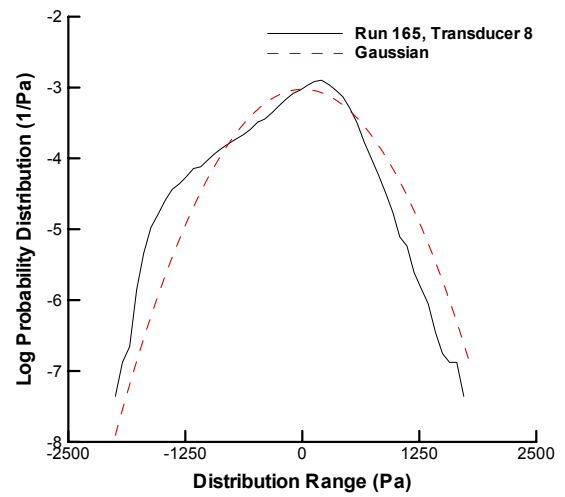


Figure 10: PDF tail of fluctuating pressure at 56mm upstream of forward-facing step.

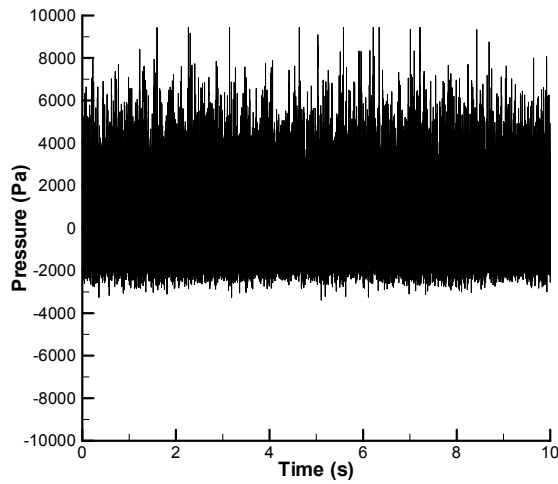


Figure 11: Fluctuating pressure time history at 1mm upstream of forward-facing step.

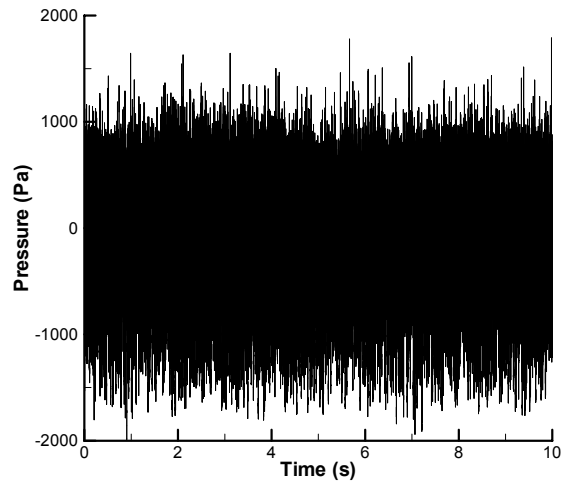


Figure 12: Fluctuating pressure time history at 56mm upstream of forward-facing step.

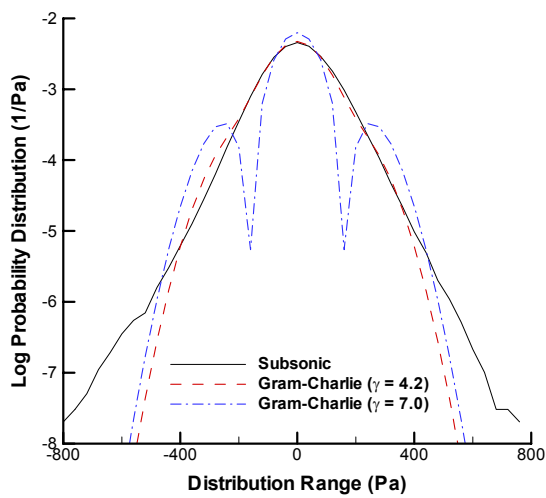


Figure 13: Gram-Charlie PDF tail of fluctuating pressure (smooth surface).

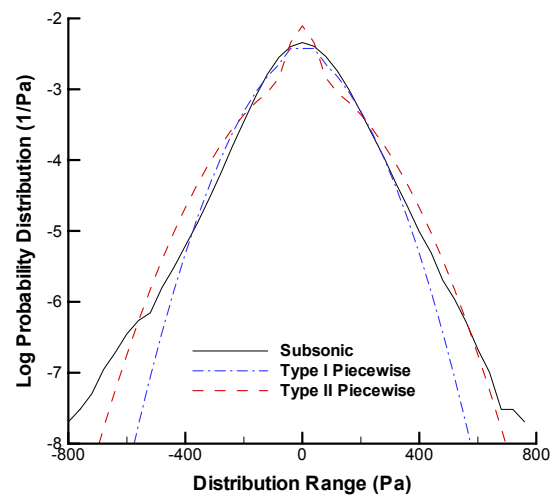


Figure 14: Piecewise-Gaussian PDF tail of fluctuating pressure (smooth surface).

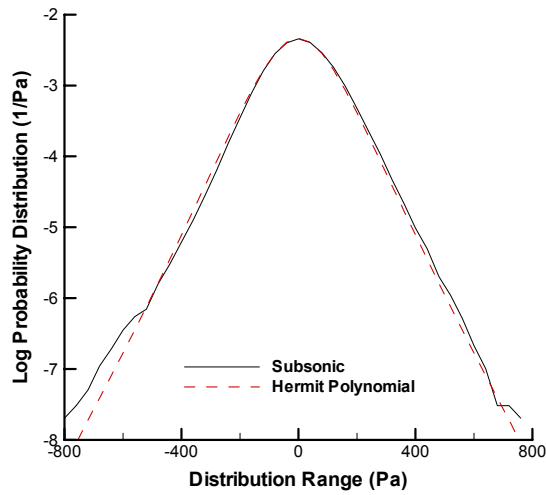


Figure 15: Hermite polynomial PDF tail of fluctuating pressure (smooth surface).

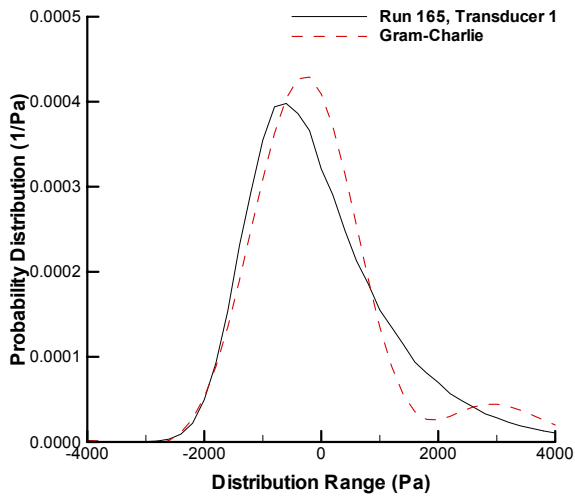


Figure 16: Gram-Charlie PDF peak of fluctuating pressure (forward step).

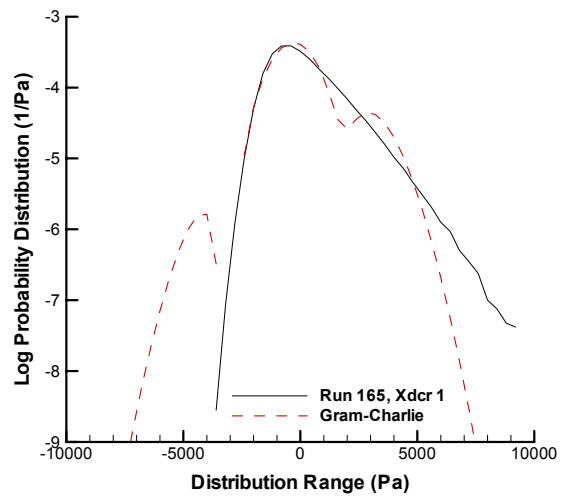


Figure 17: Gram-Charlie PDF tail of fluctuating pressure (forward step).

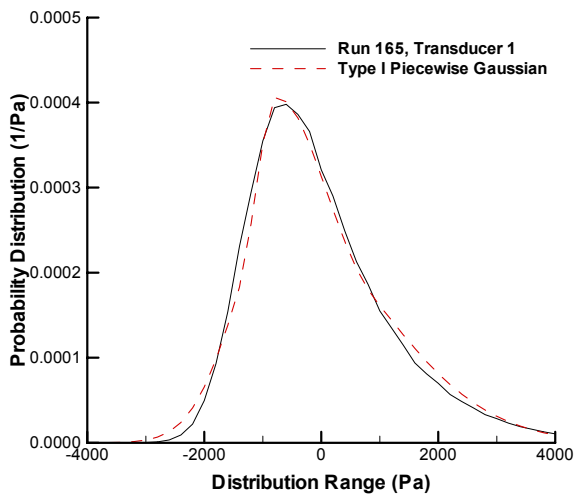


Figure 18: Type I piecewise-Gaussian PDF peak of fluctuating pressure (forward step).

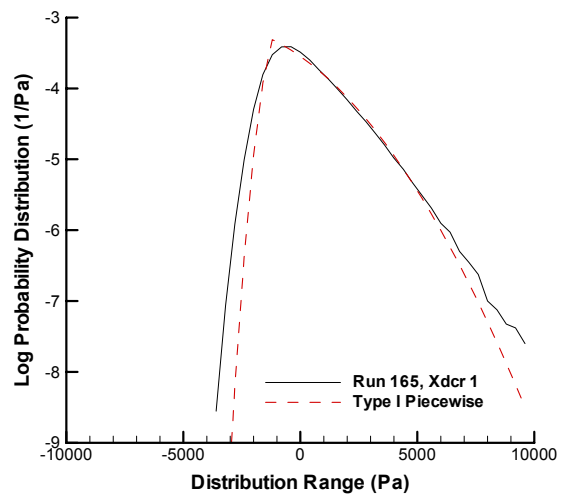


Figure 19: Type I piecewise-Gaussian PDF tail of fluctuating pressure (forward step).

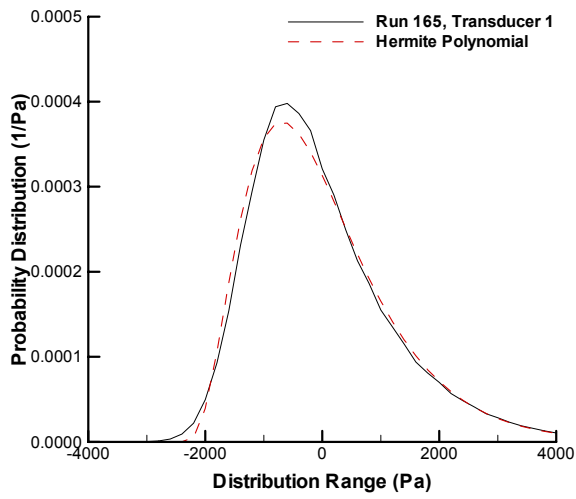


Figure 20: Hermite polynomial PDF peak of fluctuating pressure (forward step).

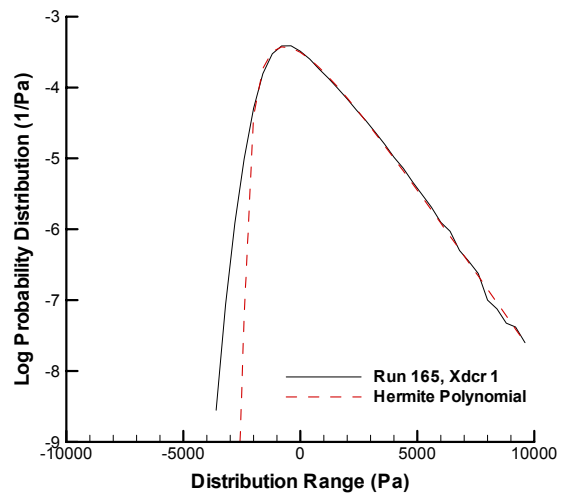


Figure 21: Hermite polynomial PDF tail of fluctuating pressure (forward step).